J. Fluid Mech. (1987), *vol.* 178, *pp.* 99–117
Printed in Great Britain

Reflection of a shallow-water soliton. Part 2. Numerical evaluation

By N. SUGIMOTO, Y. KUSAKA AND T. KAKUTANI
Department of Mechanical Engineering, Faculty of Engineering Science, Osaka University, Toyonaka, Osaka 560, Japan

(Received 10 April 1986 and in revised form 25 August 1986)

Reflection of a shallow-water soliton at a plane beach is investigated numerically based on the edge-layer theory developed in Part 1 of this series. The offshore behaviour in the shallow-water region is first obtained by solving the Boussinesq equation under the 'reduced' boundary condition. The spatial and temporal variations of the surface elevation are displayed for two typical values of the inclination angle of the beach. Using these solutions, the nearshore behaviour is then evaluated to obtain the surface elevation and the velocity distribution in the edge layer. Both offshore and nearshore behaviours furnish a full knowledge of the reflection problem of a shallow-water soliton. To check the applicability of the edge-layer theory, a 'computational experiment' is carried out based on the boundary-element method, in which the Laplace equation is solved numerically under the *full* nonlinear boundary conditions at the free surface without introducing the edge-layer concept. Both results show a fairly good agreement for the overall reflection behaviour of a shallow-water soliton except for the surging movement at the shoreline.

1. Introduction

This paper deals with a numerical study of a reflection problem of a shallow-water soliton at a sloping plane beach based on the edge-layer theory developed in Part 1 (Sugimoto & Kakutani 1984; hereinafter referred to as I). The edge-layer theory consists of two parts; one dealing with the offshore behaviour and the other the nearshore behaviour. As far as the offshore behaviour is concerned, the reflection problem is dramatically simplified by the concept of the edge layer. In fact, the 'reduced' boundary condition obtained in I reflects a complicated nearshore behaviour in a compact form without loss of essential features and makes it possible to reduce the reflection problem to a boundary-value problem for the Boussinesq equation.

On the other hand, the nearshore behaviour such as a shoaling process can be obtained just after the offshore behaviour has been clarified. The numerical calculation is carried out for the inclination angle $\theta = \frac{1}{6}\pi$ and $\theta = \frac{1}{15}\pi$ with the wave height-to-depth ratio $\alpha = 0.07$. As was remarked in I, the behaviour in the edge layer is 'linear' because the horizontal dimension of the beach region is too narrow for the nonlinearity assumed in the shallow-water region to accumulate. Within the linear theory, therefore, the surging movement of the shoreline along the beach surface cannot be described, only an elevation (which we regard as the maximum 'run-up' in the linear theory) at the quiescent shoreline can be calculated. This may cast doubt on the validity of the linear theory near the shoreline. However, we are satisfied with the endorsement by the theory of full nonlinear shallow-water waves near the

shoreline which states that its exact regular solution approaches a (regular) linear one for a sufficiently small amplitude (Carrier & Greenspan 1958).

In order to confirm the applicability of the edge-layer theory, a 'computational experiment' is carried out based on the boundary-element method developed in diverse applications (for example, Jaswon & Symm 1977; Brebbia 1984) and particularly devised for a run-up problem by Kim, Liu & Liggett (1983). Without introducing any physical simplification such as the edge-layer concept, the Laplace equation is solved numerically over the whole region under the *full* nonlinear boundary conditions at the free surface. Numerical results thus obtained are displayed separately for the shallow-water region and for the nearshore region to facilitate a qualitative and quantitative comparison with the results obtained by the edge-layer theory. Due to the exact treatment of the boundary conditions at the free surface, the surging movement of the shoreline is now explicitly obtained so that the actual maximum run-up (the vertical elevation at the surging-up shoreline) can be calculated. Except for this surging movement, the edge-layer theory gives fairly good results for the overall reflection behaviour of a shallow-water soliton.

2. Summary of the edge-layer theory

In this section, we summarize the main results of the edge-layer theory developed in I and, in part, extend them to incorporate higher-order terms. Unless otherwise stated, the same notation as in I will be used throughout. We consider two-dimensional and irrotational wave motion of an inviscid fluid in a constant-depth shallow-water region that extends semi-infinitely in the positive x-direction and is bounded by a plane beach with an inclination angle θ at one end. The origin of the coordinate x is assumed to be at the toe of the slope and the beach is assumed to extend over a narrow region $-x_s < x < 0$, where $-x_s$ is the position of the shoreline at the still water level and $x_s \lesssim O(1)$.

By taking account of the weak effects of both the nonlinearity and dispersion, a behaviour in the offshore shallow-water region is assumed to be described by the Boussinesq equation for the velocity potential f in the lowest approximation:

$$f_{tt} - f_{xx} - \tfrac{1}{3}\beta f_{xxtt} = -\alpha(f_t f_{xx} + 2 f_x f_{xt}) + O(\alpha^2, \alpha\beta, \beta^2), \dagger \tag{2.1}$$

where the free-surface elevation η is given by

$$\eta = -f_t - \tfrac{1}{2}\alpha f_x^2 + \tfrac{1}{2}\beta f_{ttt} + O(\alpha\beta, \beta^2). \tag{2.2}$$

In the above equations, the horizontal coordinate x and the time t are normalized, respectively, by a characteristic wavelength l and a characteristic time $l/(gh)^{\frac{1}{2}}$, where h is the constant depth in the shallow-water region and g is the acceleration due to gravity, while f is normalized by $agl/(gh)^{\frac{1}{2}}$, a being a characteristic wave elevation from the still-water level; the subscripts denote partial differentiation with respect to the indicated variable. Here we recall that the small parameter $\alpha\,(= a/h)$ measures weak nonlinearity while $\beta\,(= (h/l)^2)$ measures weak dispersion.

† In this series of papers, equation (2.6) in I is referred to as the Boussinesq equation which is of a form capable of describing bi-directional wave propagation. For derivation of (2.1), see Whitham (1974), Miles (1977) and Wu (1981). In the corresponding expression (2.6) in I, we omitted α^2 in $O(\alpha\beta, \beta^2)$. The nonlinear term $\frac{1}{2}(f_t^2)_t$ in (2.6) in I has been replaced equivalently by $f_t f_{xx}$ in (2.1) by using the fact $f_{tt} \approx f_{xx} + O(\alpha, \beta)$. The latter is preferable in connection with the numerical calculations and the higher-order Boussinesq equation discussed in Appendix A.

From the edge-layer theory in I (cf. (4.7) in I), it was found that the 'reduced' boundary condition relevant to (2.1) is given by

$$f_x = \mu f_{xx} - \tfrac{1}{2}\mu^2 f_{xxx} + \tfrac{1}{6}\mu^3 f_{xxxx} + O(\mu^5, \beta) \quad \text{at } x = 0, \tag{2.3}$$

where $\mu = x_s (= \xi_0 \text{ in I}) = \beta^{\frac{1}{2}} \cot\theta \lesssim O(1)$. For small values of μ of $O(\beta^{\frac{1}{2}})$, it is sufficient to consider only the first term on the right-hand side of (2.3). However, as μ becomes larger, the higher-order terms of μ must be included in (2.3). Here note that the second and the third terms on the right-hand side are of comparable order of magnitude because $f_{xxx} \approx f_{xtt}$ and $f_{xxxx} \approx f_{xxtt}$, while $f_x \approx \mu f_{xx}$ in the lowest approximation of (2.3). At any rate, it is this 'reduced' boundary condition that reduces the reflection problem to a boundary-value problem for (2.1) to be solved in the shallow-water region $x > 0$.

On the other hand, the nearshore behaviour can be described by the edge-layer solution. The boundary value of the velocity potential ϕ_∞ and that of the surface elevation η_∞ at the matching region ($\xi \to \infty$ but $x \to 0$) between the edge-layer and the outer shallow-water region are given by

$$\phi_\infty = f + \beta^{\frac{1}{2}} f_x \xi + \tfrac{1}{2}\beta f_{xx}(\xi^2 - z^2) + \tfrac{1}{6}\beta^{\frac{3}{2}} f_{xxx}(\xi^3 - 3\xi z^2) + \tfrac{1}{24}\beta^2 f_{xxxx}(\xi^4 - 6\xi^2 z^2 + z^4) + O(\mu^5), \tag{2.4a}$$

$$\eta_\infty = -f_t - \beta^{\frac{1}{2}} f_{xt}\xi - \tfrac{1}{2}\beta f_{xxt}(\xi^2 - 1) - \tfrac{1}{6}\beta^{\frac{3}{2}} f_{xxxt}(\xi^3 - 3\xi) - \tfrac{1}{24}\beta^2 f_{xxxx}(\xi^4 - 6\xi^2 + 1) - \tfrac{1}{2}\alpha f_x^2 + O(\mu^5, \mu\alpha), \tag{2.4b}$$

which correspond to (3.5a) and (3.5b) in I respectively. In the above expressions, $\xi (= \beta^{-\frac{1}{2}} x)$ and z imply, respectively, the horizontal and vertical coordinates in the edge layer, both normalized by h. In (2.4a, b), we have retained the terms of a higher-order with respect to μ than those in (3.5a, b) in I (note that $\xi = -\cot\theta$ at the shoreline), in order to apply (2.4a, b) to a fairly large value of μ such that $O(\beta^{\frac{1}{2}}) < \mu < O(1)$. In the context of the edge-layer theory, f and its derivatives with respect to x and t are known functions of time t determined from the solution of the Boussinesq equation at $x = 0$.

For a plane beach given by $\xi = b(z) = -(\cot\theta)\, z$, the boundary condition (4.6) in I reads as

$$2f_x(\psi_\xi + \cot\theta \psi_z) = -f_x + 2\mu f_{xx} z - \tfrac{3}{2}\mu^2 f_{xxx} z^2 + \tfrac{2}{3}\mu^3 f_{xxxx} z^3 + O(\mu^4, \beta), \tag{2.5}$$

where $\psi = \psi(\xi, z, t)$ denotes the deviation of the velocity potential $\phi(\xi, z, t)$ in the edge layer from the boundary value ϕ_∞ (cf. (3.7) in I):

$$\phi = \phi_\infty + 2\beta^{\frac{1}{2}} f_x \psi. \tag{2.6}$$

Upon using the 'reduced' boundary condition (2.3) to eliminate f_{xxxx} in (2.5), the integral expression of the edge-layer solution ψ takes the following form:

$$\left.\begin{aligned} f_x \psi(\xi, z, t) &= -\int_{-1}^{1} G(\zeta_r', 0; \zeta_r, \zeta_i)\, K[z'(\zeta_r')] \frac{dz'}{d\zeta_r'} d\zeta_r', \\ \text{with} \quad \frac{dz'}{d\zeta_r'} &= -\frac{1}{\pi} \sin\theta (1 - \zeta_r')^{-1/m} (1 + \zeta_r')^{1/m - 1}, \\ K(z') &= \mu f_{xx}(z' - \tfrac{1}{2}) + 2(f_x - \mu f_{xx})(z'^3 - \tfrac{1}{4}) + \mu^2 f_{xxx}(z'^3 - \tfrac{3}{4} z'^2), \\ \text{and} \quad G(\zeta_r', \zeta_i'; \zeta_r, \zeta_i) &= \frac{1}{2\pi} \log |(\zeta' - \zeta)(\zeta' - \zeta^*)|, \end{aligned}\right\} \tag{2.7}$$

which correspond to (5.14a, b) in I (ζ^* being the complex conjugate of ζ), but again by retaining the higher-order terms with respect to μ. We recall that the above results hold only for a beach angle $\theta = \pi/m$, where m is a positive integer ($m \geqslant 2$). Since f_x, f_{xx}, and f_{xxx} are known functions of time, the edge-layer solution ψ in (2.7) can be obtained only by a quadrature.

Before carrying out the integration, it is instructive to understand the nature of the transformation between the complex planes Z' and ζ' via w' introduced in I:

$$Z' = -\frac{1}{\pi}\sum_{j=0}^{m-1} w_j \log(w' - w_j), \tag{2.8a}$$

with

$$w' = \left(\frac{\zeta'+1}{\zeta'-1}\right)^{1/m} \quad \text{and } w_j = \mathrm{e}^{2\mathrm{i}\theta_j}, \tag{2.8b}$$

where $Z' = \xi' + \mathrm{i}z'$, $\zeta' = \zeta'_{\mathrm{r}} + \mathrm{i}\zeta'_{\mathrm{i}}$, and the principal value of the logarithmic function is defined by considering the range $-\pi \leqslant \arg\log(\ldots) < \pi$. The asymptotic behaviour of (2.8a) as $m \to \infty$ is particularly useful for the present purpose even if m takes relatively small values such as $m \approx 10$. Noticing that for large values of m, (2.8a) is nothing but the trapezoidal rule for the following integral along a unit circle in the complex plane W:

$$\frac{Z'}{m} \sim \frac{\mathrm{i}}{2\pi^2}\oint \log(w' - W)\,\mathrm{d}W + O(m^{-2}), \tag{2.9}$$

the asymptotic behaviour of Z' can be evaluated with the aid of Cauchy's integral theorem. Much attention must be paid, however, to the location of w' because $W = w'$ is a branch point. If w' is located outside the circle, that is, $|w'| > 1 + O(m^{-1})$, the integral (2.9) vanishes so that the outside region is mapped into the region near the origin of Z'. If w' is located inside the circle, that is, $|w'| < 1 - O(m^{-1})$, on the other hand, the evaluation of (2.8a) must be carefully done because the branch cut for the logarithmic function necessarily crosses the unit circle. Introducing the cut in the W-plane as shown in figure 1, the summation (2.8a) is rearranged as

$$\begin{aligned} Z' = -\frac{1}{\pi}\Big[&\tfrac{1}{2}\log(w' - w_0) + \tfrac{1}{2}w_{m-1}\log(w' - w_{m-1}) + \tfrac{1}{2}\log(w' - w_0) \\ &+ \tfrac{1}{2}w_{m-1}\log(w' - w_{m-1}) + \sum_{j=1}^{m-2} w_j \log(w' - w_j)\Big]. \end{aligned} \tag{2.10}$$

Except for the first two terms, all the terms can be replaced asymptotically by the contour integral along an open unit circle C from $W = w_0 (= 1)$ to $W = w_{m-1}$. When the auxillary contour C' starting from $W = w_{m-1}$ to $W = w_0$, partly along the unit circle and partly along the branch cut shown in figure 1, is introduced, the original integral along C is equivalently replaced by that along C' (with the sign reversed). Evaluation of the latter by the trapezoidal rule leads to

$$Z' - \left(\frac{-m}{\pi} + \mathrm{i}\right) = \frac{mw'}{\pi} + O(m^{-1}). \tag{2.11}$$

This asymptotic relation states that the wedge region of w' shown in figure 4 in I inside the unit circle corresponds to the region in the Z'-plane near the shoreline without any distortion except the uniform expansion due to the factor m/π. The unit circle $|w'| = 1$ separating the above two regions corresponds to the imaginary axis in the ζ'-plane (figure 3 in I), which corresponds to the curve in the Z'-plane (figure 2 in I) starting from a definite point on the beach ($-\pi^{-1}\log 2, \mathrm{i}m^{-1}\log 2$) and extending

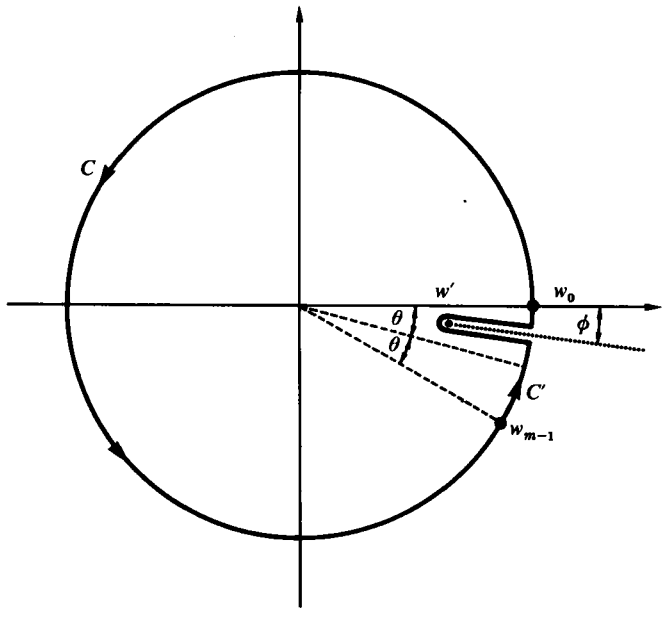

FIGURE 1. Complex W-plane where the cut is introduced from $W = w' = |w'|e^{-i\phi}(0 < \phi < \theta = \pi/m)$ to infinity along the straight line on which arg $W = -\phi$. Contour C is an open unit circle starting from w_0 to w_{m-1}, while C' is a part of the unit circle starting from w_{m-1} to w_0 with the detour along the branch cut.

monotonically towards infinity $(\infty, \frac{1}{2}i)$. The remaining narrow strip region in w' spreading around $|w'| = 1$ with a width of $O(m^{-1})$ corresponds to the region in the Z'-plane on both sides of the curve corresponding to $|w'| = 1$.

From the definition of ζ' in (2.8*b*), on the other hand, the region, except in the neighbourhood of $\zeta' = -1$ and $\zeta' = 1$, is mapped on to a region very close to $|w'| = 1$ as $m \to \infty$. In other words, only the two regions extremely near $\zeta' = -1$ and $\zeta' = 1$ correspond, respectively, to the inside and outside regions of the unit circle $|w'| = 1$. Although the beach in the Z'-plane, i.e. $\xi' = -(\tan\theta)z'$, corresponds to the real axis $|\zeta'_r| < 1$ in the ζ'-plane, the major part of the beach is closely packed near the point $\zeta' = -1$. This correspondence is given asymptotically by

$$w' \sim e^{-i\theta}[\tfrac{1}{2}(\zeta' + 1)]^{1/m}. \tag{2.12}$$

From both relations (2.11) and (2.12), the major part of the beach is given by

$$Z' - \left(\frac{-m}{\pi} + i\right) = \frac{m e^{-i\theta}[\frac{1}{2}(\zeta' + 1)]^{1/m}}{\pi}. \tag{2.13}$$

This result suggests that when the integral in (2.7) is carried out with respect to ζ'_r, the main contribution comes from the narrow region near $\zeta'_r = -1$. Thus the numerical integration is carried out by dividing the interval $(-1, 1)$ into small intervals, whose length is decreased exponentially toward $\zeta'_r = -1$, and further on subdividing each small interval by equally spaced points to apply Simpson's rule.

After evaluating ψ, the elevation η is obtained from (3.10*b*) in I as

$$\eta = \eta_\infty - 2\beta^{\frac{1}{2}}(f_x \psi)_t \quad \text{at } z = 1, \tag{2.14}$$

while the velocity components are calculated by differentiating the velocity potential

(2.6) with respect to ξ and z. In the latter process, the derivatives of $f_x\psi$ are evaluated by the following integrals:

$$f_x\begin{bmatrix}\psi_\xi\\ \psi_z\end{bmatrix} = -\int_{-1}^{1}\begin{bmatrix}-\zeta_r'+\zeta_r & \zeta_i\\ \zeta_i & \zeta_r'-\zeta_r\end{bmatrix}\begin{bmatrix}R\\ I\end{bmatrix}\frac{K[z'(\zeta_r')]}{(\zeta_r'-\zeta_r)^2+\zeta_i^2}\frac{\mathrm{d}z'}{\mathrm{d}\zeta_r'}\mathrm{d}\zeta_r', \tag{2.15}$$

where $\zeta(=\zeta_r+\mathrm{i}\zeta_i)$ is a point $\zeta'=\zeta$ corresponding to $Z'=Z(=\xi+\mathrm{i}z)$ through the transformation (2.8*a*, *b*); R and I are defined by the real and imaginary parts of the inverse of the Schwarz–Christoffel transformation (5.3) in I:

$$R+\mathrm{i}I=\frac{1}{\pi}\frac{\mathrm{d}\zeta}{\mathrm{d}Z}=(\zeta+1)^{1-1/m}(\zeta-1)^{1/m}. \tag{2.16}$$

3. Results of the edge-layer theory

Let us first investigate the offshore behaviour in the shallow-water region by solving the Boussinesq equation (2.1) under the condition (2.3). It is numerically solved here by an implicit finite-difference method. Although we are interested in reflection of a soliton incident from infinity to shoreward, we are obliged technically to introduce another 'numerical' boundary located at $x=L$, say, far enough from the one at $x=0$. Hence the reflection problem is posed as an initial-boundary-value problem in such a way that a soliton initially located at $x=C(0\ll C\ll L)$ is pushed shoreward as if it were propagated from $x=\infty$. The surface elevation of a single soliton solution with unit peak propagating shoreward with a constant speed λ is given by

$$\eta=\operatorname{sech}^2[D(x+\lambda t-C)], \tag{3.1}$$

with $\lambda=1+\frac{1}{2}\alpha$, and $D=[3\alpha/(4\beta\lambda^2)]^{\frac{1}{2}}$. To derive (3.1), we have used the following steady-progressive-wave solution for the velocity potential f:

$$f=-\frac{1}{\lambda D}\tanh[D(x+\lambda t-C)], \tag{3.2}$$

discarding terms of $O(\alpha,\beta)$. In this regard, we remark on the accuracy of the approximation involved in the shallow-water theory. Equations (2.1) and (2.2) might appear to give a correction to the linear theory up to $O(\alpha,\beta)$ inclusive. But f is specified only within the order of unity, since $f_{tt}-f_{xx}=(\lambda^2-1)f_{xx}=O(\alpha)$ and the terms of $O(\alpha^2,\alpha\beta,\beta^2)$ have been neglected. Therefore, in order to specify η up to $O(\alpha,\beta)$ inclusive, f should be specified up to $O(\alpha,\beta)$ as well. To do so, the neglected terms of $O(\alpha^2,\alpha\beta,\beta^2)$ in (2.1) must be retained. In Appendix A, we give this higher-order correction to the Boussinesq equation (2.1), by which η can be obtained up to $O(\alpha,\beta)$ correctly. We note that the refined result agrees perfectly with that of the second-order approximation for the solitary wave obtained by Laitone (1960). Hence we emphasize again that when (2.1) is used as a basic approximate equation in the shallow-water region, it should be kept in mind that f (and therefore η) cannot be evaluated from (2.1) alone up to the terms of $O(\alpha,\beta)$ correctly. In this connection, as was mentioned in the concluding remarks in I, it should also be emphasized that the boundary condition (2.3) gives a fairly large correction of $O(\beta^{\frac{1}{2}})$ to the shallow-water region or even a correction of nearly $O(1)$ when $\theta\lesssim\beta^{\frac{1}{2}}$, although we have to take account of the higher-order terms of μ when $\theta\lesssim\beta^{\frac{1}{2}}$.

To solve (2.1) under (2.3), the numerical values of α and β must be specified. If we take the initial maximum elevation of the soliton as the characteristic elevation, α is naturally defined, whereas the value of β is not so obvious as that of α since the

characteristic length l is ambiguous. Unlike a periodic wavetrain, no obvious wavelength is defined for a soliton, so that an 'effective' wavelength has to be defined. Since the coordinate x has already been normalized by this ambiguous length l, the unit length in x corresponds to l. In other words, the horizontal spread of the elevation (3.1) at which η takes the value η_r ($= \mathrm{sech}^2(\frac{1}{2}D)$) also corresponds to the length l. Since the elevation (3.1) expressed by the sech^2-function has a slimmer form than a sech-function, we choose $\eta_r = \mathrm{sech}^2(\frac{1}{2}D) = \frac{1}{4}$, i.e. $\mathrm{sech}(\frac{1}{2}D) = \frac{1}{2}$ rather than $\eta_r = \frac{1}{2}$. Then $D\,(= [3\alpha/(4\beta\lambda^2)]^{\frac{1}{2}} \doteqdot [3\alpha/(4\beta)]^{\frac{1}{2}})$ takes the value 2.63 so that the Ursell parameter (Ursell 1953) takes the value $\alpha/\beta = U_r \doteqdot 9.25$ (we note incidentally that in most experiments, the Ursell parameter U_r takes larger values, between about 10 and 40, since a longer l is usually taken). Thus once α is chosen, β is automatically determined by $\beta = \alpha/U_r \doteqdot 0.108\alpha$. Since the value of the Ursell parameter thus chosen is rather large, there arises the question of whether the neglected term of $O(\alpha^2)$ in (2.1) might be comparable with the retained term of $O(\beta)$. Therefore, in the following calculation, we modify (2.1) so as to include the term $\frac{3}{2}\alpha^2 f_x^2 f_{xx}$ (see Appendix A). In accordance with this modification, similar corrections for the initial condition are also made by taking the higher-order effect of α into account.

For the choice of suitable values for parameters α and θ, we show in figure 2 experimental data, where the inclination angle θ together with the slope $\tan\theta$ is taken as the abscissa and α and β as the ordinate. The solid straight lines represent the constant-μ lines. The left-hand upper portion above $\mu = 1.0$ corresponds to a 'gentle' slope, while the right-hand lower portion corresponds to a 'steep' slope in the sense that the horizontal dimension of the beach is less than one characteristic wavelength. Since the edge-layer theory, as formulated in I, assumes a 'steep' beach, we are concerned here with the parameters lying on the line $\mu \lesssim O(1)$. The experimental results obtained by Ippen & Kulin (1955) and the theoretical one by Peregrine (1967) for 'gentle' slopes ($\mu > O(1)$) are also included for comparison. It was revealed in I that the effect of the beach appears to the shallow-water region only through a factor $\mu = \beta^{\frac{1}{2}}\cot\theta$ contained in the 'reduced' boundary condition. Interestingly enough, it was reported by Pedersen & Gjevik (1983) that the run-up height for a solitary wave is crucially determined by the parameter $\alpha^{\frac{1}{2}}\cot\theta$, where α is again the wave height-to-depth ratio. Since the parameters α and β are assumed to be of comparable order of magnitude, $\alpha^{\frac{1}{2}}\cot\theta$ is equivalent to $\beta^{\frac{1}{2}}\cot\theta$ except for the square root of the Ursell parameter. Recalling $\beta^{\frac{1}{2}} = h/l$, however, $\beta^{\frac{1}{2}}\cot\theta\,(= h\cot\theta/l)$ has rather an appealing physical significance because it indicates the ratio of the horizontal dimension of the beach to the characteristic wavelength, which indicates to what depth a soliton penetrates into the beach region.

In choosing the parameters α and θ, we must notice one more important point. Since the present theory does not presuppose wave breaking, we are concerned here with a perfect reflection only. Many authors have given criteria for breaking of waves climbing up a plane beach, but the identification of breaking depends crucially on observers so that criteria do not seem to be firmly established. Amongst them, we refer here to two non-breaking conditions for a plane beach, one obtained by Street & Camfield (1966) and the other by Gjevik & Pedersen (1981) (see also Pedersen & Gjevik 1983). The former indicates that for an inclination of beach $\theta > 0.18\,(= 10.3°)$, solitary waves surge up the beach surface without breaking, irrespective of the magnitude of wave height-to-depth ratio α. The latter indicates that the wave breaking during backwash occurs for $\alpha > 0.48(\tan\theta)^{\frac{10}{9}}$. In figure 2, the broken line represents the breaking criterion obtained by Street & Camfield (1966) and the chain line shows the breaking criterion $\alpha = 0.48(\tan\theta)^{\frac{10}{9}}$ by Gjevik & Pedersen (1981). In the

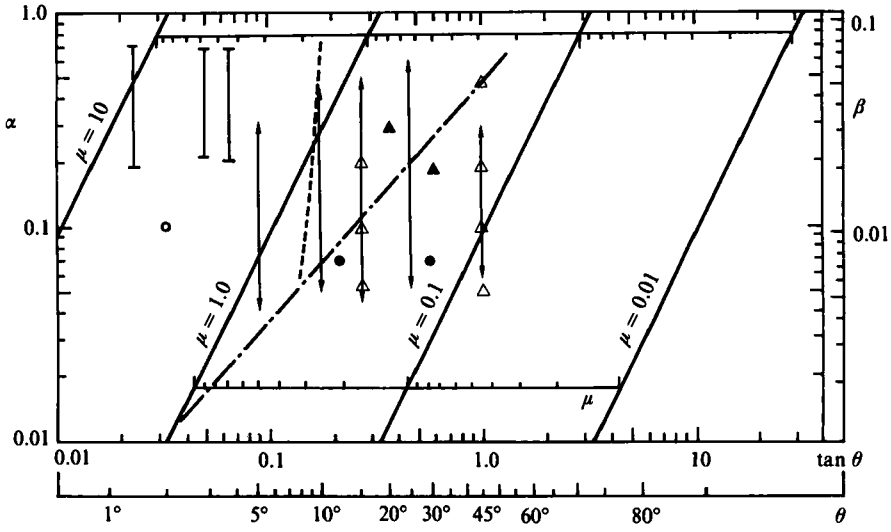

FIGURE 2. The diagram for initial wave height-to-depth ratio $\alpha (= a/h)$, dispersion parameter $\beta (= (h/l)^2)$, and inclination of the beach surface $\tan\theta$. The solid straight lines represent constant-μ lines, while broken and chain lines represent, respectively, the breaking criteria obtained by Street & Camfield (1966) and by Gjevik & Pedersen (1981). Several experimental and theoretical results so far obtained are marked together with the present calculations (Ursell parameter $U_r = \alpha/\beta = 9.25$) where different symbols ($\updownarrow$, Hall & Watts 1953; $\downarrow$, Ippen & Kulin 1955; ○, Peregrine 1967; △, Kim *et al.* 1983; ▲, Pedersen & Gjevik 1983; ●, present calculations) are used for respective results.

following, we choose two typical sets of parameters α and θ, $(\alpha = 0.07, \theta = \frac{1}{6}\pi)$ and $(\alpha = 0.07, \theta = \frac{1}{15}\pi)$, to demonstrate a difference owing to the values of μ. For the former choice, μ takes the value 0.15 which is about twice the value of $\beta^{\frac{1}{2}} = 0.087$ but comparable with it, while for the latter, μ takes a fairly large value of $\mu = 0.41$ significantly larger than $O(\beta^{\frac{1}{2}})$.

Figures 3(*a*) and 4(*a*) show the spatial and temporal variations of the surface elevation in the shallow-water region for $\theta = \frac{1}{6}\pi$ and $\theta = \frac{1}{15}\pi$, respectively. The numerical scheme to solve the initial-boundary-value problem for the Boussinesq equation is given in Appendix B. Taking the shallow-water region bounded by the 'numerical' boundary at $x = L = 4.0$ where $f_x = 0$, we have assumed that the initial soliton be located at $x = C = 2.0$. It is, of course, more interesting to take L wider than 4.0 in order to investigate long-time evolution of a soliton after reflection. But L is chosen here as narrow as possible because the main purpose of this paper is to confirm the applicability of the edge-layer theory. For the purpose of comparison with the 'computational experiment', L cannot be taken so large that the pursuit of the long-time evolution in the shallow-water region is beyond the present scope. The right-hand parts of figures 3(*a*) and 4(*a*) show the spatial variations over the shallow-water region $0 \leqslant x \leqslant L$ at several times for $0 \leqslant t \leqslant 5.0$. On the other hand, the left-hand parts show the temporal variation of the surface elevation observed at $x = 0$ for $0 \leqslant t \leqslant 5.0$. It is found that for $\theta = \frac{1}{6}\pi$, the soliton is reflected back without any apparent change in waveform, whereas for $\theta = \frac{1}{15}\pi$, the soliton is subjected to a substantial change. In the left-hand of figure 3(*a*), the peak indicated by the arrow *c* takes 1.69 at $t = 2.09$. In the left-hand of figure 4(*a*), by contrast, two peaks indicated by the arrows *b* and *f* appear. The former peak has the value 1.15 at $t = 1.98$, while the latter 0.974 at $t = 2.85$, which may be interpreted, respectively,

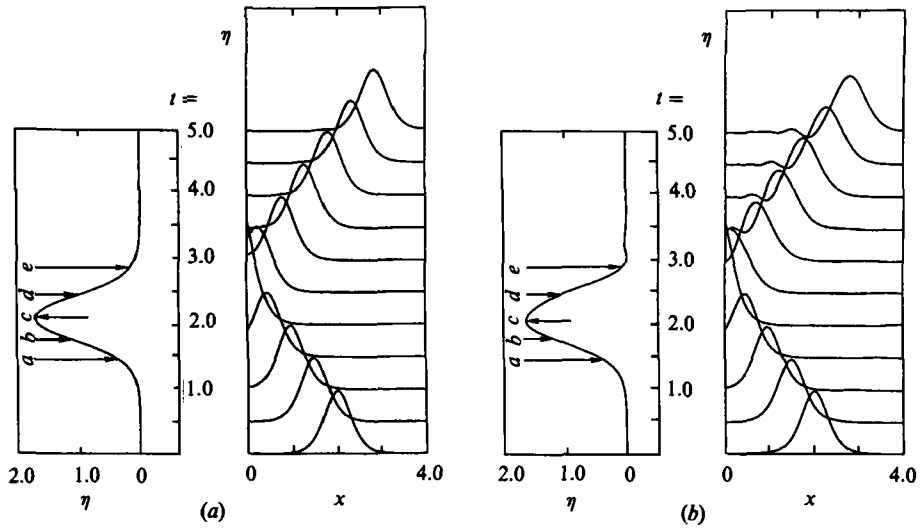

FIGURE 3. Comparison of the spatial and temporal variations of the surface elevation in the shallow-water region due to (*a*) the edge-layer theory (*b*) the BEM for $\theta = \frac{1}{6}\pi$ and $\alpha = 0.07$; arrows *a*–*e* in (*a*) and (*b*) correspond to the timesteps *a*–*e* shown in figures 5 and 8, respectively.

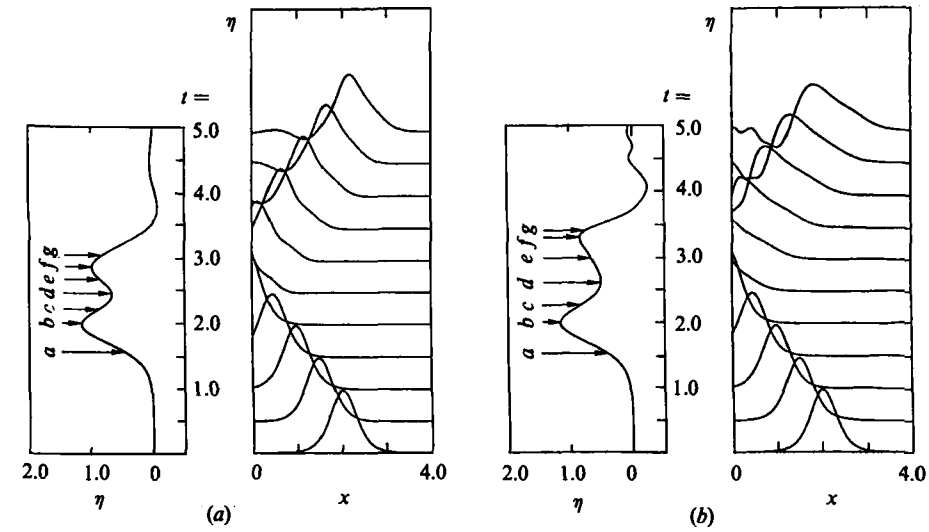

FIGURE 4. Comparison of the spatial and temporal variations of the surface elevation in the shallow-water region due to (*a*) the edge-layer theory (*b*) the BEM for $\theta = \frac{1}{15}\pi$ and $\alpha = 0.07$; arrows *a*–*g* in (*a*) and (*b*) correspond to the timesteps *a*–*g* shown in figures 6 and 9, respectively.

as the soliton passing shoreward and that passing seaward after reflection at the actual beach. The difference in the number of peaks at $x = 0$ results naturally from the magnitude of μ. It is conjectured that as μ increases, i.e. the beach region becomes wider, the soliton would stay there for a longer period and therefore the two peaks for the incident and reflected soliton would tend to be separated. For $\theta = \frac{1}{6}\pi$, however, the beach region is so narrow that two peaks almost overlap each other.

Now that the boundary values of f and their derivatives at $x = 0$ are available from the solution of the Boussinesq equation, we can proceed to obtain the nearshore behaviour in the edge layer. Using those data to evaluate ϕ_∞ and η_∞ in (2.4*a*, *b*) and

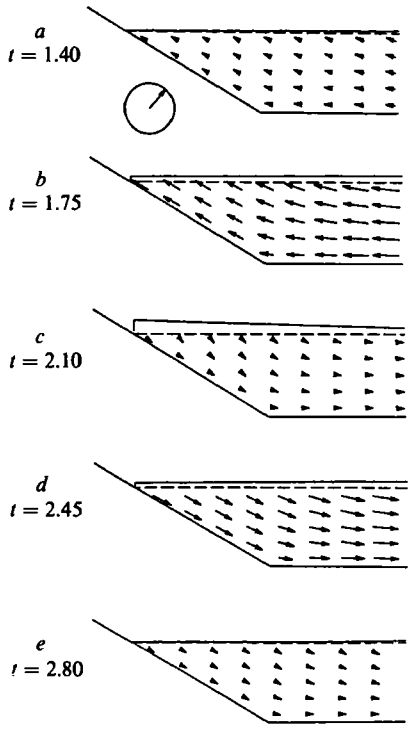

FIGURE 5. Nearshore behaviour calculated by the edge-layer theory; temporal variations of the surface elevation and the velocity field for $\theta = \frac{1}{6}\pi$ and $\alpha = 0.07$, where the small circle at the top measures the reference velocity vector with its magnitude 0.05 and the broken line represents the still-water level. The timesteps *a–e* correspond to the times shown in figure 3(*a*).

carrying out the integration in (2.7) numerically, we can obtain the edge-layer solution ψ. Then (2.6) and (2.14) give the velocity potential and the surface elevation, respectively. Figures 5 and 6 show the surface elevation and the velocity vectors (ϕ_ξ, ϕ_z) at representative points in the edge layer for $\theta = \frac{1}{6}\pi$ and $\theta = \frac{1}{15}\pi$, respectively. In figure 5, the timesteps *a–e* chosen corresponds, respectively, to those indicated by the arrows *a–e* in figure 3(*a*). This figure shows an explicit nearshore behaviour, how the soliton rushes to the beach and retreats seaward. At the timestep *c*, the movement of the water almost vanishes in the edge layer. As mentioned in §1, the surface elevation cannot be obtained beyond the quiescent shoreline, i.e. $\xi < -\cot\theta$. The maximum 'run-up' at this point is attained at $t = 2.10$ (which is slightly larger than $t = 2.09$ when the maximum surface elevation occurs at $x = 0$) with its ratio 2.39 to the incident soliton. This ratio is somewhat larger than the experimental value 2.27 observed by Hall & Watts (1953). Figure 6 shows the similar nearshore behaviour for $\theta = \frac{1}{15}\pi$. The timesteps *a–g* chosen correspond to those indicated by the arrows *a–g* shown in figure 4(*a*). The detailed discussion on this figure will be given in §4 in connection with the results of the 'computational experiment' described there. Here we only make the following brief remark. The maximum 'run-up' is attained in this case at $t = 2.35$ with its ratio 3.95 to the incident soliton. This result shows an over-estimation compared with the experimental maximum run-up 2.95 observed by Hall & Watts (1953). Nevertheless it is rather surprising that the edge-layer theory can give a qualitatively good result for the maximum 'run-up' in spite of its inherent rough assumption near the shoreline.

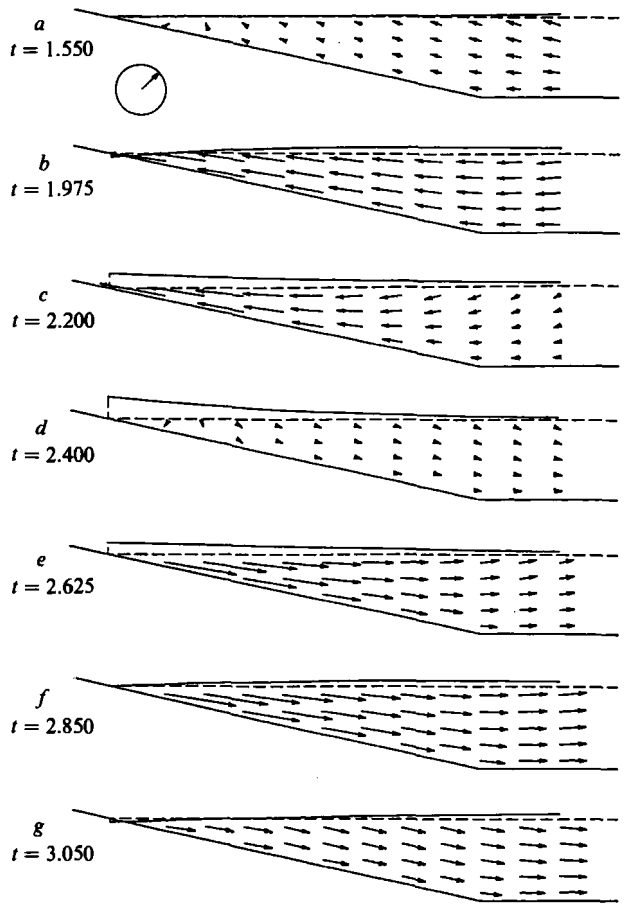

FIGURE 6. Nearshore behaviour calculated by the edge-layer theory; temporal variations of the surface elevation and the velocity field for $\theta = \frac{1}{15}\pi$ and $\alpha = 0.07$, where the small circle at the top measures the reference velocity vector with its magnitude 0.05 and the broken line represents the still-water level. The timesteps *a*–*g* correspond to the times shown in figure 4(*a*).

4. Results of the boundary-element method

To confirm the validity of the edge-layer theory developed so far, we now consider the same reflection problem by using the boundary-element method (BEM). The Laplace equation is now solved numerically over the whole region under the *full* nonlinear boundary conditions at the free surface and the free-slip condition at the beach and bottom surfaces. The numerical scheme used here is essentially the same as the one devised by Kim, Liu & Liggett (1983) for the run-up problem, but the initial and boundary conditions are different. Since Kim *et al.* were concerned only with the run-up behaviour, the shallow-water region they considered was limited to be relatively narrow and a solitary wave was generated by means of a piston-type wavemaker with a prescribed motion for a soliton. Obviously it is less efficient, in computation, to take a wide shallow-water region because of the significant difference in the horizontal lengthscales associated with the shallow-water region and the edge layer. For the purpose of comparison with the results of the edge-layer theory, however, a wider shallow-water region is desirable. As a compromise, the shallow-water region is taken here to be in $0 \leqslant x \leqslant L = 4.0$, i.e. $0 \leqslant \xi \leqslant \beta^{-\frac{1}{2}}L$.

The idea of the BEM is that the Laplace equation is not solved locally but is solved globally by its converted integral equation to be satisfied by the boundary values of ϕ and its outward normal derivatives $\partial\phi/\partial n$. This conversion to the integral equation is provided by the Green's theorem:

$$\kappa\phi(p) = \int_{\partial S}\left[\phi(q)\frac{\partial}{\partial n}\log r - \frac{\partial\phi}{\partial n}(q)\log r\right]\mathrm{d}s, \tag{4.1}$$

where $\phi(p)$ denotes symbolically a value of ϕ at a point p on the boundary ∂S of the region, while $\phi(q)$ and $\partial\phi(q)/\partial n$ denote values of ϕ and $\partial\phi/\partial n$ on the integration point q along ∂S and $\mathrm{d}s$ designates its line element; a parameter κ takes π for a regular point on ∂S but it takes an interior angle for a corner point. Here r is the distance between points p and q, and the integral in (4.1) is taken in the sense of Cauchy's principal value.

When the shape of the boundary ∂S is known, (4.1) is straightforward to solve together with the boundary conditions on ∂S. But the free surface changes its form with time according to the boundary conditions given by

$$\left.\begin{aligned} \frac{\partial\eta}{\partial t} &= \frac{1}{\beta\cos\delta}\frac{\partial\phi}{\partial n}, && (4.2a)\\ \frac{\partial\phi}{\partial t} &= -\eta - \frac{\alpha}{2\beta}\left[\left(\frac{\partial\phi}{\partial s}\right)^2 + \left(\frac{\partial\phi}{\partial n}\right)^2\right] && (4.2b) \end{aligned}\right\} \quad \text{on } z = 1+\alpha\eta,$$

where δ denotes an angle of the tangent to a surface elevation to the horizontal ($\tan\delta = \partial(\alpha\eta)/\partial\xi$) and $\partial\phi/\partial s$ stands for the derivative of ϕ along the boundary ∂S.

In the following analysis of this section, the origin of the coordinate axes ξ and z is transferred to the quiescent level at the vertical wall (introduced as the 'numerical' boundary in §3) as shown in figure 7. In order to describe the surging movement along the beach surface, the auxiliary coordinates ξ^* and z^* rotated by an angle γ are introduced. For the free surface between A and B, we choose γ in such a way that it is changed successively from zero for the point A to $\frac{1}{2}\pi-\theta$ for the point B on the beach to describe the surging movement. It should be remarked here that the introduction of ξ^* and z^* does not imply a full coordinate transformation of the independent variables in the system of equations (4.2a, b). But they are introduced only to measure η and ϕ along such an auxiliary direction. Denoting the surface elevation along z^* by $\alpha\eta^*$, the boundary conditions (4.2a, b) are transformed into

$$\left.\begin{aligned} \frac{\partial\eta^*}{\partial t} &= \frac{1}{\beta\cos(\delta-\gamma)}\frac{\partial\phi}{\partial n} && (4.3a)\\ \left(\frac{\partial\phi}{\partial t}\right)^* &= -\eta - \frac{\alpha}{2\beta}\left[\left(\frac{\partial\phi}{\partial s}\right)^2 - \left(\frac{\partial\phi}{\partial n}\right)^2 - 2\tan(\delta-\gamma)\frac{\partial\phi}{\partial s}\frac{\partial\phi}{\partial n}\right] && (4.3b) \end{aligned}\right\} \quad \text{on } z^* = \alpha\eta^*,$$

where $(\partial\phi/\partial t)^*$ stands for the time derivative of ϕ moving along the free surface with ξ^* held fixed. Here we note that at the free surface between O' and A in figure 7, γ is chosen to be zero. Once ϕ (and therefore $\partial\phi/\partial s$) and $\partial\phi/\partial n$ are known for a definite shape of the region at a fixed instant, the temporal evolution of η^* and ϕ can be calculated according to the conditions (4.3a, b).

Next we consider the initial conditions. At an initial time $t = 0$, we impose them in such a way that the peak of the soliton, as if it were steadily propagating shoreward from infinity, passes the position $\xi = C' = -\frac{1}{2}\beta^{-\frac{1}{2}}L$ located far enough from both the

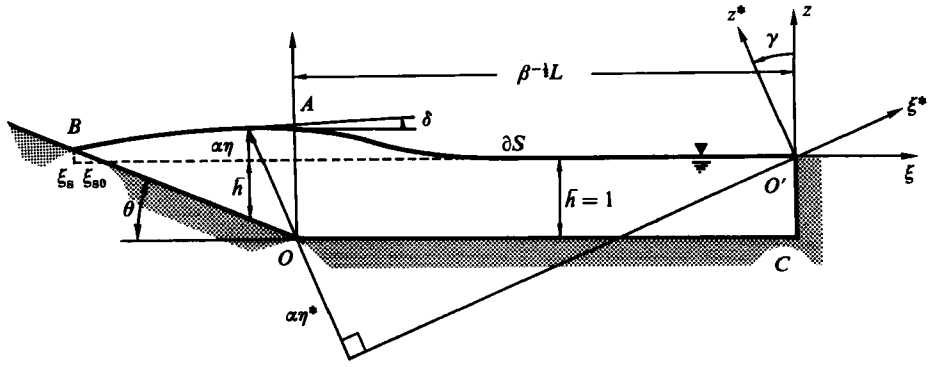

FIGURE 7. Definition of the fixed coordinate system (ξ, z) and the rotated one (ξ^*, z^*) used in the BEM, where the elevation at the points between O' and A is measured along the vertical z-direction and the elevation at the points between A and B is measured along the rotated direction z^*.

beach and the 'numerical' vertical wall. From the shallow-water soliton given in §3, the initial values for η, ϕ, and $\partial\phi/\partial n$ are taken as

$$\left.\begin{aligned} \eta &= \operatorname{sech}^2 Y, \\ \phi &= -\left(\frac{4\beta}{3\alpha}\right)^{\frac{1}{2}} \tanh Y, \\ \frac{\partial\phi}{\partial n} &= -(3\alpha\beta)^{\frac{1}{2}} \cos\delta \operatorname{sech}^2 Y \tanh Y, \end{aligned}\right\} \tag{4.4}$$

where $Y = \{3\alpha/[4(1+\alpha)]\}^{\frac{1}{2}}(\xi - C')$ and $\partial\phi/\partial n$ is calculated by (4.2a).

In the numerical computations, the boundary ∂S of the region is divided into five large segments, $O'A$, AB, BO, OC, and CO', each of which is further subdivided into 80, 10, 10, 38, and 10 equally spaced small intervals, respectively. Discretizing the integral equation (4.1) by the boundary values for ϕ and $\partial\phi/\partial n$ at the end points of the intervals, (4.1) is reduced to a set of simultaneous algebraic equations, which is complemented by the boundary conditions (4.3a, b) at the free surface and the free-slip condition ($\partial\phi/\partial n = 0$) at the beach and the bottom surfaces. Discretizing time by finite differences with an increment of 0.05, a new shape of the free surface is calculated by (4.3a, b) after imposing the boundary values at the end points. Since (4.3a, b) are nonlinear, their evaluation is not so straightforward. We use an iteration scheme until convergence for η, ϕ, and $\partial\phi/\partial n$ is achieved with the relative error of less than 1 %. Such a technique for iteration is the same as that used by Kim *et al.* (1983); refer to their paper for the detailed discussion.

To check the numerical accuracy of the computations, the total excess volume Q and the excess energy E defined below are always monitored at each timestep:

$$Q = \int_{\xi_s}^{0} (\alpha\eta + \bar{h})\,\mathrm{d}\xi - \int_{\xi_{s0}}^{0} \bar{h}\,\mathrm{d}\xi, \tag{4.5a}$$

and

$$E = \frac{1}{2}\left[\frac{\alpha^2}{\beta}\oint \phi\frac{\partial\phi}{\partial n}\,\mathrm{d}s + \int_{\xi_s}^{0} (\alpha^2\eta^2 - \bar{h}^2)\,\mathrm{d}\xi + \int_{\xi_{s0}}^{0} \bar{h}^2\,\mathrm{d}\xi\right], \tag{4.5b}$$

where ξ_s and ξ_{s0} denote, respectively, the horizontal position of the changing shoreline and the quiescent level; $\bar{h}$ is the still-water depth normalized by the uniform depth

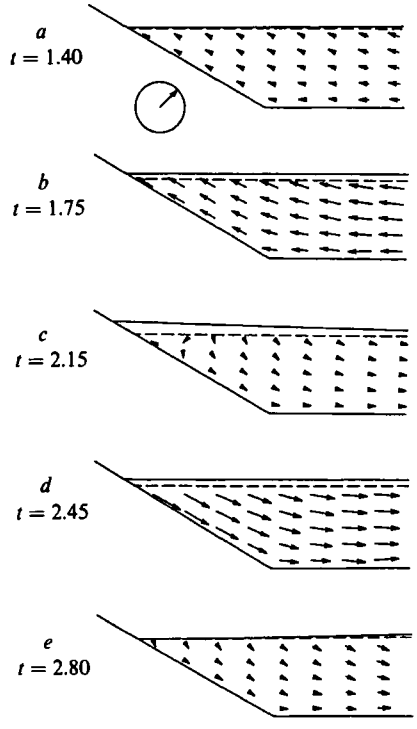

FIGURE 8. Nearshore behaviour calculated by the BEM; temporal variations of the surface elevation and the velocity field for $\theta = \frac{1}{6}\pi$ and $\alpha = 0.07$, where the small circle at the top measures the reference velocity vector with its magnitude 0.05 and the broken line represents the still-water level. The timesteps *a–e* correspond to the times shown in figure 3(*b*).

h. Incidentally, Kim *et al.* (1983) have neither imposed the convergence conditions for ϕ and $\partial\phi/\partial n$ nor checked the conservation of the total excess volume and energy.

To compare with the results of the edge-layer theory, the results of the BEM are displayed separately for the shallow-water region and for the nearshore region. Figures 3(*b*) and 4(*b*) show, respectively, the behaviour of the surface elevation in the shallow-water region for $\theta = \frac{1}{6}\pi$ and for $\theta = \frac{1}{15}\pi$, which should be compared with that based on the edge-layer theory shown in figures 3(*a*) and 4(*a*). In each figure, the right-hand side shows the spatial variations of the surface elevation from $t = 0$ to $t = 5.0$, while the left-hand side shows their temporal variations at $x = 0$. For $\theta = \frac{1}{6}\pi$, both the waveforms shown in figures 3(*a*, *b*) appear to be almost the same except for the small hump behind the main wave in figure 3(*b*). The peak in the surface elevation at $x = 0$ takes 1.69 at $t = 2.09$ in figure 3(*a*), while it takes 1.63 at $t = 2.05$ in figure 3(*b*). In the right-hand side of figures 4(*a*, *b*) for $\theta = \frac{1}{15}\pi$, both the reflected waveforms appear to be similar but not identical. In the result of the BEM, the phase shifts behind that of the edge-layer theory after the reflection (the reason for this will be discussed later). It is also observed that the maximum elevation obtained by the BEM is slightly lower than that of the edge-layer theory and the width of the main wave is slightly wider. Behind the main wave, there are commonly observed small depression regions but no rapid oscillating humps are found in the result of the edge-layer theory.

In the temporal variation of the surface elevation at $x = 0$ shown in the left-hand side of figure 4(*b*), two peaks are also observed; the first peak *b* has the value 1.15 at $t = 2.00$, while the second one *f* has the value 0.840 at $t = 3.30$. As conjectured

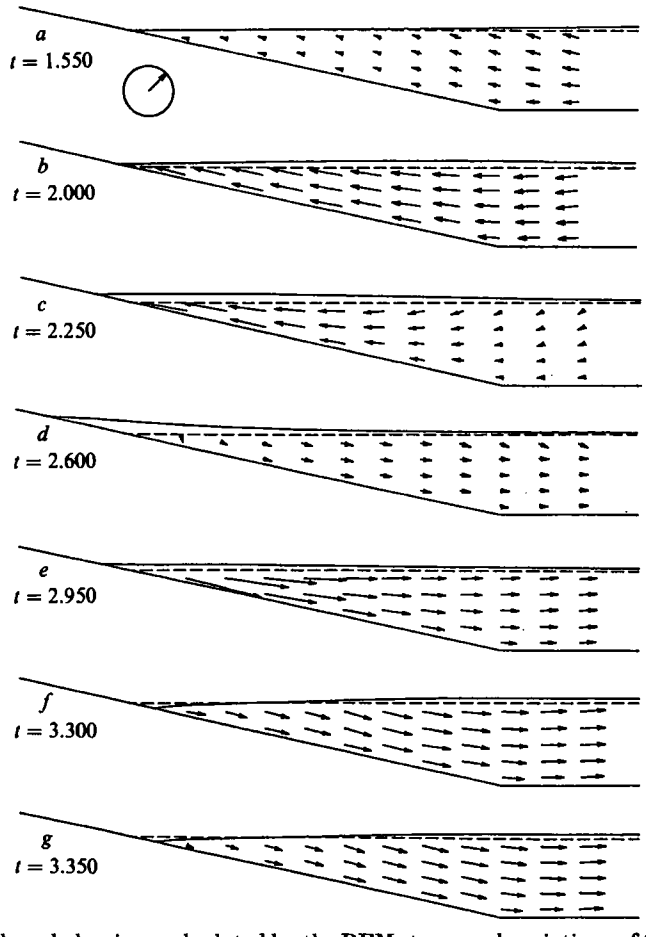

FIGURE 9. Nearshore behaviour calculated by the BEM; temporal variations of the surface elevation and the velocity field for $\theta = \frac{1}{15}\pi$ and $\alpha = 0.07$, where the small circle at the top measures the reference velocity vector with its magnitude 0.05 and the broken line represents the still-water level. The timesteps *a*–*g* correspond to the times shown in figure 4 (*b*).

in §3, the first peak corresponds to the incident soliton passing shoreward, while the second to the one passing seaward after the reflection at the beach. Therefore it is naturally supposed that the maximum run-up is attained during a time between the two peaks, probably at a time when η is minimum (*d*), which will turn out to be the case. By comparing the results of the BEM with those of the edge-layer theory, it is rather surprising to see that the elevations and the occurring times of the first peak show a very good quantitative agreement. For the second peak, however, the elevation in the case of the BEM is slightly lower and subjected to a time lag, which is clearly consistent with the phase shift appearing in the spatial variations.

Next, let us consider the nearshore behaviour. Figures 8 and 9 show the surface elevation and the velocity vectors for $\theta = \frac{1}{6}\pi$ and $\theta = \frac{1}{15}\pi$, respectively, chosen at the corresponding points in figures 5 and 6 based on the edge-layer theory. To obtain the velocity components in the interior region, (4.1) with $\kappa = 2\pi$ is differentiated with respect to ξ and z, respectively. We note here that the interpolated boundary values for ϕ and $\partial\phi/\partial n$ have been used. Due to the exact treatment of the free surface, the surging movement can now be explicitly calculated. The timesteps *a*–*e* chosen in

figure 8 correspond to the ones indicated by the arrows *a–e* shown in figure 3(*b*), where the maximum surface elevation at $x = 0$ occurs at $t = 2.05$. The elevation and the velocity vectors in figure 8 appear to be almost the same as those in figure 5 except for the actual surging movement. The maximum run-up is attained at $t = 2.15$ with its ratio 2.29 to the incident soliton. This ratio gives a slightly larger value than the experimental one of 2.27 observed by Hall & Watts (1953), but less than the one of 2.39 obtained by the edge-layer theory.

In figure 9, the timesteps *a–g* chosen correspond to the ones indicated by the arrows *a–g* shown in figure 4(*b*). The arrows *b* and *f* indicate the timesteps for the maximum elevation at $x = 0$ due to the incident soliton and the reflected soliton, respectively, while *d* indicates the timestep for the minimum elevation at $x = 0$ and *g* corresponds to a timestep for the minimum run-down at the shoreline to be observed. Although each time indicated by *a–g* in figures 6 and 9 is not identical, overall nearshore behaviours are very similar to each other except for the actual surging movement. It is this surging movement, however, that is responsible for the phase shift observed in the shallow-water behaviour calculated by the BEM. Because the shoreline runs up along the beach, the effective horizontal dimension of the beach is slightly wider than the one fixed in the edge-layer theory so that the soliton stays at the beach for a longer period. This produces a substantial phase shift in the shallow-water region. The maximum run-up takes the ratio 3.09 at $t = 2.60$ to the incident soliton, which should be compared with 3.95 at $t = 2.35$ obtained from the edge-layer theory. In the BEM, the time $t = 2.60$ for the maximum run-up agrees perfectly with the time when the surface elevation at $x = 0$ becomes minimum (arrow *d* in figure 4*b*). In the edge-layer theory, however, both times are slightly different; the time for the maximum 'run-up' is observed at $t = 2.35$ whereas the time for the minimum elevation at $t = 2.44$.

Finally we mention the results about the conservation of total excess volume and energy (4.5*a*, *b*). It is found that, for both the cases with $\theta = \frac{1}{6}\pi$ and $\theta\frac{1}{15}\pi$, the excess volume is always conserved within a relative error sufficiently less than 1 %. On the other hand, the energy is almost conserved within a relative error of 1 % for $\theta = \frac{1}{6}\pi$, whereas it decreases by several per cent for $\theta = \frac{1}{15}\pi$ when $t > 3.25$.

5. Conclusion

We have demonstrated how the edge-layer theory can be applied effectively to the reflection problem of a shallow-water soliton at a sloping beach. It is found that the 'reduced' boundary condition, in spite of its simple form, can give a substantial effect of the beach on the Boussinesq equation which was originally proposed to describe shallow-water waves on an infinitely extended layer with uniform depth. According to the result due to the BEM shown in figure 4(*b*), it is not so striking to observe that two peaks appearing in the surface elevation at $x = 0$ correspond to the peaks of the incident and reflected solitons. But in the edge-layer theory, it is rather surprising to see that such a simple 'reduced' boundary condition can give the two peaks fairly correctly. For the nearshore behaviour, however, the edge-layer theory has an inherent drawback incapable of describing the actual surging movement along the beach surface. Nevertheless it is supported by the BEM that it can qualitatively describe the nearshore behaviour except for this surging movement. Thus it may be concluded that the edge-layer theory can give a qualitatively adequate result for the overall reflection problem of a shallow-water soliton.

The authors would like to express their thanks to the editor and the referees for a number of comments and suggestions. They also acknowledge Daikin Comtec Inc., Osaka, Japan for the instrumental support of the computer graphics. All the computations were carried out on the NEC Acos-system 1000 of the Computer Centre of Osaka University.

Appendix A. Higher-order correction to the Boussinesq equation

Here we briefly give the results for the higher-order correction to the Boussinesq equation (2.1) by retaining the neglected terms of $O(\alpha^2, \alpha\beta, \beta^2)$. Following the same procedure as shown in §2 of I and retaining the neglected terms, we have the higher-order Boussinesq equation which gives the correct result for η in (2.2) up to $O(\alpha, \beta)$:

$$f_{tt}-f_{xx}-\tfrac{1}{3}\beta f_{xxtt}+\alpha f_t f_{xx}+2\alpha f_x f_{xt}+\tfrac{3}{2}\alpha^2 f_x^2 f_{xx}+\tfrac{1}{6}\alpha\beta[f_t f_{xx}+(f_x^2)_t]_{xx} +\tfrac{1}{4}\alpha\beta(f_t^2)_{tt}-\alpha\beta(f_x f_{xt})_t-\tfrac{1}{45}\beta^2 f_{xxtttt}=O(\alpha\beta^2, \alpha^2\beta, \beta^3). \quad \text{(A 1)}$$

If one seeks a progressive-wave solution of f in the form of $f(x+\lambda t)=f(X)$ and uses (2.2), the higher-order soliton solutions are obtained as

$$\left.\begin{aligned} f &= -\frac{1}{\lambda D}[1-\tfrac{1}{4}\alpha+\tfrac{1}{3}\alpha\tanh^2(DX)]\tanh(DX)+\ldots, \\ \text{and}\quad \eta &= \operatorname{sech}^2(DX)-\tfrac{3}{4}\alpha\operatorname{sech}^2(DX)\tanh^2(DX)+\ldots, \\ \text{with}\quad \lambda &= \pm(1+\tfrac{1}{2}\alpha-\tfrac{3}{20}\alpha^2+\ldots), \\ \text{and}\quad D^2 &= \frac{3\alpha}{4\beta}(1-\tfrac{5}{4}\alpha+\ldots), \end{aligned}\right\} \quad \text{(A 2)}$$

which agree perfectly with the result of the second-order theory for a solitary wave obtained by Laitone (1960).

Appendix B. Implicit finite-difference scheme to solve the Boussinesq equation

First we divide the bounded-space region into N equally spaced intervals with length $\Delta x = L/N$ and also discretize the time by a small interval Δt. Denoting $f(x,t)$ at each mesh point by $f(I\Delta x, J\Delta t)=f(I,J)$ simply, I and J being integers, we approximate (2.1) by using the second-order central-difference formulae. Then we have the following difference equation that approximates (2.1) with the correction term $\frac{3}{2}\alpha^2 f_x^2 f_{xx}$:

$$\begin{aligned} &[-\beta'+\alpha'\Delta t\, g(I,J)]f(I+1,J+1)+[(\Delta x)^2+2\beta'+2\alpha'\Delta t\, h(I,J)]f(I,J+1) \\ &\quad+[-\beta'-\alpha'\Delta t\, g(I,J)]f(I-1,J+1) \\ &\quad=(\Delta x)^2[2f(I,J)-f(I,J-1)]+(\Delta t)^2 h(I,J)+\beta'[h(I,J-1)-2h(I,J)] \\ &\quad+\alpha'\Delta t[2f(I,J-1)h(I,J)+g(I,J)g(I,J-1)]-6\alpha'^2(\Delta t/\Delta x)^2 g(I,J)^2 h(I,J), \end{aligned} \quad \text{(B 1}a\text{)}$$

where $g(I,J)$ and $h(I,J)$ are defined as

$$g(I,J)=f(I+1,J)-f(I-1,J), \quad \text{(B 1}b\text{)}$$

$$h(I,J)=f(I+1,J)-2f(I,J)+f(I-1,J), \quad \text{(B 1}c\text{)}$$

and $\alpha'=\frac{1}{4}\alpha$ and $\beta'=\frac{1}{3}\beta$.

Next we consider the boundary conditions. At the sloping beach $x = 0$, we use (2.3), whereas at the 'numerical' boundary $x = L$, we simply impose $f_x = 0$ for a 'vertical beach', since the boundary condition at $x = L$ is not so important as the one at $x = 0$. To approximate the boundary condition (2.3) and the one at $x = L$, we introduce two fictitious points $f(-1, J)$ and $f(N+1, J)$ outside the region concerned. Then the boundary condition (2.3) and the one at $x = L$ are approximated by

$$\begin{aligned}(1+s+3s'+9s'')f(-1,J) &= (2s+10s'+42s'')f(0,J)+(1-s-12s'-79s'')f(1,J)+(6s'+76s'')f(2,J)\\ &\quad -(s'+39s'')f(3,J)+10s''f(4,J)-s''f(5,J), \qquad \text{(B 2)}\end{aligned}$$

and

$$f(N+1,J) = f(N-1,J), \qquad \text{(B 3)}$$

respectively, where $s = 2\mu/\Delta x$, $s' = \mu^2/[2(\Delta x)^2] = \frac{1}{8}s^2$, and $s'' = \mu^3/[12(\Delta x)^3] = \frac{1}{96}s^3$, and f_{xxx} and f_{xxxx} are evaluated, respectively, by biased five-point and seven-point finite-difference formulae:

$$f_{xxx} = \frac{-3f(-1,J)+10f(0,J)-12f(1,J)+6f(2,J)-f(3,J)}{2(\Delta x)^3}, \qquad \text{(B 4}a\text{)}$$

$$f_{xxxx} = \frac{9f(-1,J)-42f(0,J)+79f(1,J)-76f(2,J)+39f(3,J)-10f(4,J)+f(5,J)}{4(\Delta x)^4}. \qquad \text{(B 4}b\text{)}$$

On the other hand, the initial condition for $f(I, 0)$ is given by the right-hand side of (3.2) with $t = 0$ and $x = I\Delta x$. To push the soliton shoreward, we impose another condition that $f(I, -1)$ should be given by the right-hand side of (3.2) with $t = -\Delta t$ and $x = I\Delta x$. The higher-order corrections to these conditions are given by (A 2). Thus provided $f(I, J-1)$ and $f(I, J)$ $(0 < J, -1 \leqslant I \leqslant N+1)$ are known up to J, (B 1), (B 2), and (B 3) give $N+3$ implicit relations among $f(I, J+1)$. Using the Gaussian elimination method, we solve these simultaneous equations stepwise to obtain numerical solutions.

Checking the condition of linear stability for the present numerical scheme, it is found that Δx and Δt must satisfy the condition

$$(\Delta t)^2 - (\Delta x)^2 \leqslant \tfrac{4}{3}\beta. \qquad \text{(B 5)}$$

Therefore if Δt is chosen to be equal to Δx, the scheme is unconditionally stable for the linear problem. But we note that this condition does not take account of the effects of the boundaries. Finally we note that N in the present calculations is taken to be 320 so that $\Delta x = \Delta t = 0.0125$ for $L = 4.0$.

REFERENCES

Brebbia, C. A. (ed.) 1984 *Topics in Boundary Element Research*, vol. 1. Springer.

Carrier, G. F. & Greenspan, H. P. 1958 Water waves of finite amplitude on a sloping beach. *J. Fluid Mech.* **4**, 97–109.

Gjevik, B. & Pedersen, G. 1981 Run-up of long waves on an inclined plane. *Preprint Series Institute of Mathematics*, University of Oslo.

Hall, J. V. & Watts, G. M. 1953 Laboratory investigation of the vertical rise of solitary waves on impermeable slopes. *US Army, Corps of Engrs, Beach Erosion Board, Tech. Memo* no. 33. (cited in R. L. Wiegel 1964 *Oceanographical Engineering*. Prentice-Hall).

Ippen, A. T. & Kulin, G. 1955 The shoaling and breaking of the solitary wave. In *Proc. 5th Conf. Coastal Engng*, pp. 27–47.

JASWON, M. A. & SYMM, G. T. 1977 *Integral Equation Methods in Potential Theory and Elastostatics.* Academic.

KIM, S. K., LIU, P. L-F. & LIGGETT, J. A. 1983 Boundary integral equation solutions for solitary wave generation, propagation and run-up. *Coastal Engng* **7**, 299–317.

LAITONE, E. V. 1960 The second approximation to cnoidal and solitary waves. *J. Fluid Mech.* **9**, 430–444.

MILES, J. W. 1977 Obliquely interacting solitary waves. *J. Fluid Mech.* **79**, 157–169.

PEDERSEN, G. & GJEVIK, B. 1983 Run-up of solitary waves. *J. Fluid Mech.* **135**, 283–299.

PEREGRINE, D. H. 1967 Long waves on a beach. *J. Fluid Mech.* **27**, 815–827.

STREET, R. L. & CAMFIELD, F. E. 1966 Observations and experiments on solitary wave deformation. In *Proc. 10th Conf. Coastal Engng*, pp. 284–301.

SUGIMOTO, N. & KAKUTANI, T. 1984 Reflection of a shallow-water soliton. Part 1. Edge layer for shallow-water waves. *J. Fluid Mech.* **146**, 369–382.

URSELL, F. 1953 The long-wave paradox in the theory of gravity waves. *Proc. Camb. Phil. Soc.* **49**, 685–694.

WHITHAM, G. B. 1974 *Linear and Nonlinear Waves.* Wiley-Interscience.

WU, T. Y. 1981 Long waves in ocean and coastal waters. *J. Engng Mech. Div. ASCE* **107**, 501–522.